ELSEVIER

Contents lists available at ScienceDirect

Acta Biomaterialia

journal homepage: www.elsevier.com/locate/actbio



Scale performance and composition in a small Amazonian armored catfish, *Corydoras trilineatus*



Andrew Lowe^a, Adam P. Summers^b, Ryan P. Walter^a, Sean Walker^a, E.W. Misty Paig-Tran^{a,*}

- ^a Department of Biological Science (MH-282), California State University, Fullerton, 800 N State College Blvd, Fullerton, CA, 92834-6850, USA
- ^b University of Washington's Friday Harbor Laboratories, Friday Harbor, WA, 98250, USA

ARTICLE INFO

Article history: Received 11 July 2020 Revised 19 October 2020 Accepted 24 November 2020 Available online 30 November 2020

Keywords: Corydoras trilineatus mechanical properties armor

ABSTRACT

The cory catfishes (Callichthyidae) are small, South American armored catfishes with a series of dermal scutes that run the length of the fish from posterior to the parieto-supraoccipital down to the caudal peduncle. In this study, we explore the anatomy and functional performance of the armored scutes in the three-striped cory catfish, Corydoras trilineatus. The lateral surface has a dorsal and a ventral row of scutes that interact at the horizontal septum. The scutes have little overlap with sequential posterior scutes (~33% overlap) and a deep ridge in the internal surface that connects to the underlying soft tissue. The internal surface of C. trilineatus scutes is stiffer than the external surface, contrary to the findings in a related species of cory catfish, C. aeneus, which documented a hypermineralized, enamel-like, noncollagenous, hyaloine layer along the external surface of the scute. Clearing and staining of C. trilineatus scutes revealed that the scutes have highly mineralized (~50% mineralization) regions embedded in between areas of low mineralization along the posterior margin. Puncture tests showed that posterior scutes were weaker than both anterior and middle scutes, and scutes attached to the body required 50% more energy to puncture than isolated scutes. Corydoras trilineatus has the strongest armor in areas critical for protecting vital organs and the external armored scute receives synergistic benefits from interactions to the soft underlying tissue, which combine to provide a tough protective armor that still allows for flexible mobility.

Statement of significance

Our study investigated the anatomy and performance (mineralization, imbrication, and puncture resistance) of scutes in a small, armored catfish. The scutes make use of overlapping connections with adjacent scutes reinforced by a deep, internal, mineralized ridge. The mineralization varies across the scute with lower mineralization occurring in areas of overlap while the highest degree of mineralization is found in the central portion of the scute. These tiny fishes can withstand up to four Newtons of puncture force. To put this into context, these fish are five orders of magnitude less massive than a famous armored fish, piracuru, but withstand just two orders of magnitude less force. In other words, their puncture resistance is quite impressive for their size.

© 2020 Acta Materialia Inc. Published by Elsevier Ltd. This is an open access article under the CC BY-NC-ND license (http://creativecommons.org/licenses/by-nc-nd/4.0/)

1. Introduction

Dermal armor is found in every major group of vertebrates, including fishes, amphibians, squamates, archosaurs, and mammals. Armor spans geologic time scales, from 400 million years ago to extant animals, and sizes - from fishes less than 3 centimeters long to dinosaurs more than 30 m long [1-11]. Armor comes in a variety of forms ranging in composition from dense cortical

^{*} Corresponding author at: Department of Biological Science (MH-282), California State University, Fullerton, 800 N State College Blvd, Fullerton, CA, 92834-6850, USA.

E-mail addresses: alowe@csu.fullerton.edu (A. Lowe), fishguy@uw.edu (A.P. Summers), rwalter@fullerton.edu (R.P. Walter), swalker@fullerton.edu (S. Walker), empaig-tran@fullerton.edu (E.W. Misty Paig-Tran).

bone to lightweight keratin and structures including: plates (Placoderms) [1], osteoderms (dinosaurs, crocodiles, turtles, etc.) [2-10], and scales (pangolins, extant fishes) [2,3,11]. In extant fishes, scales are usually composed of stacked layers of Type I collagen fibers arranged in a Bouligand pattern, reinforced by a superficial, collagen-deficient, enamel-like, capping layer that is hypermineralized and hardened by hydroxyapatite and connected by a network of collagen fibers that provide additional mechanical reinforcement [12-19].

Fishes with scales range in size from 2 to 350 cm (standard length, SL) [20-28] and scales are classified into four major categories: placoid, cosmoid, ganoid, and elasmoid [15,18,29], the composition of which varies greatly. For example, placoid scales (dermal denticles) are comprised of ectomesodermal scales anchored into the underlying stratum compactum via Sharpey fibers [30]. The scales do not overlap, instead they are separated via skin tissue [30]. The surface of the scale is covered in a dentine layer with an acellular basal plate and an underlying pulp cavity surrounded by a layer of dentine [18]. Cosmoid scales (ex. ancient Sarcopterygians) were composed of layers of dentine and spongy bone capped by vitrodentine without a core pulp [15,18]. Ganoid scales (ex. alligator gars (Atractosteus spatula) [27] and adult Senegal bichirs (Polypterus senegalus)) [23,24] are composed of rigid, jointed plates connected by a peg-and-socket joint. The plates are composed of two layers - a thin hyper-mineralized ganoine layer that covers a vascularized dentine plate and an underlying thick parallel-fibered bony basal plate [31]. Most extant fishes, including the piracuru (Arapaima gigas) [25], striped bass (Morone saxatilis) [26], and extant Sarcopterygians, the coelacanth (Latimeria chalumnae) [20-21] and lungfish (Neoceratodus forsteri) [22], are covered by elasmoid scales - thin, imbricating scales consisting of a bony surface and fibrous collagen layers capped by a hypermineralized layer called the "limiting layer" [15,18]. Elasmoid scales are separated into two subcategories: cycloid and ctenoid scales. Ctenoid scales (ex. coelacanth, striped bass and other Perciformes) have spiny denticulated structures - ctenii (tubular dentine with enameloid on the tip) - protruding from the posterior surface of the scales. Cycloid scales (ex. A. gigas, salmon - Oncorhynchus sp., and many carp: Cyprinidae) lack the posterior denticulated protrusions [15].

Several families of fishes (including the armored catfishes: Loricariidae, Doradidae, and Callichthyidae and members of several orders: Siluriformes, Gasterosteiformes, Syngnathiformes, Scorpaeniformes, Tetraodontiformes) have modified elasmoid scales that form thick, rigid bony scutes [18]. Scutes differ from ganoid and elasmoid scales in that these other scales have odontogenic origins, while scutes are osteogenic in origin [18]. Scutes have layers of collagen fibers forming cellular bone and are covered by hypermineralized layers (hyaloine) either superficially (Callichthyidae and Doradidae) or in sandwiched layers (Loricariidae) [18,32]. The three-striped cory catfish, Corydoras trilineatus, is a small (2-6.1 cm SL), benthopelagic, armored catfish (Callichthyidae) of shallow streams and rivers in South America, ranging from the Peruvian Amazon to the central Amazon River basin in Brazil and Colombia to the coastal rivers of Suriname [33-35]. The armor in this genus comprises two rows (dorsal and ventral) of partially overlapping scutes that run the length of the fish [36]. Corydoras' scutes resemble both ganoid and placoid scales in structure; the scutes have a hypermineralized external surface similar to both types of scales, there are two closely connected layers (similar to ganoid scales), and they contain posteriorly located denticles (odontodes) complete with a pulp cavity surrounded by a dentine cone (similar to placoid scales) [18,37]. The scutes are composed of a collagenous, woven bony base with half of the posterior external surface covered by a layer of hyaloine - a hypermineralized, enamel-like,

non-collagenous tissue that is not present in larger armored fishes like A. gigas [18].

The goals of this study are five-fold: 1) describe the anatomy of the hard tissue that makes up the defensive armor; 2) determine the mineral content and degree of overlap in *Corydoras* scutes for comparison to other, larger fishes; 3) measure the puncture resistance of scutes in situ on freshly euthanized fishes as a real world performance metric for the armor; 4) quantify the effect of multiple scutes and soft tissue support on the mechanics of puncture to reveal the functional contributions of structure; and 5) qualitatively assess puncture damage to compare to damage seen in other fish armor.

2. Materials and Methods

The twenty-nine Corydoras trilineatus used for this study (2.1-3.4 cm standard length) were obtained from pet stores in Orange County, California, and online at PetSolutions.com and maintained in one 151 L (40-gallon) aquarium breeder tank (dimensions 92.7 cm x 48.9 cm x 43.5 cm) using a freshwater aquarium filtration system (Marineland ML90750 Magniflow Canister 220 Filter). The C. trilineatus were fed daily with food appropriate for bottomfeeding aquarium fish (dry shrimp pellets from API Fishcare). The water was kept at 24-27°C using two Aqueon 100-watt heaters per tank, and at a pH between 7.0 and 8.0 using Aqueon Water Conditioner and API pH Down, conditions similar to the natural habitat of C. trilineatus and other cohabitating Corydoras [38,39]. Corydoras trilineatus specimens were euthanized prior to puncture tests by submersion in buffered MS-222 (tricaine methanesulphonate) of at least 98% purity (1% of body weight – lethal dosage: 300-400 ppm) with water from the aquarium housing the C. trilineatus. Upon euthanization, the standard length of *C. trilineatus* was measured. All experiments complied with the guidelines of the California State University, Fullerton Institutional Animal Care and Use Committee under protocol number 17-R-03.

2.1. Computed Tomography (CT) Scanning

One specimen was CT scanned with a Bruker 1173 microsource CT scanner after fixation in formalin. The scan was made at 133kV and 66uA at a resolution of 13.1 um with a 1mm aluminum filter to attenuate soft x-rays. The projections were reconstructed with NRecon (Bruker) and visualized with 3D Slicer software (V. 4.10.2).

2.2. Composition of Armor

2.2.1. Bone ash mineralization

Seven *C. trilineatus* were used for bone ash content tests to characterize the mineral, organic, and water composition of the scutes. Scutes from the dorsal and ventral rows were removed from the anterior, middle, and posterior regions of one side of the body (left or right). Herein anterior scutes always refer to scutes 2-6, middle scutes refer to scutes 9-15, and posterior scutes refer to scutes 19-23. Scutes were extracted using a scalpel to gently sever the connecting Sharpey's fibers and underlying connective tissue deep to the posterior sides of both the target scute(s) and the scute directly anterior to the target scute(s). Fine forceps were used to lift the scute(s) from the body.

Bone ash tests were performed to determine the wet mass (water content) and dry mass (mineral content) of the scute, as a percentage of the initial dry weight. Each scute was placed in an aluminum foil cup and weighed to the nearest microgram. Bone ash content of scutes was obtained through the same process used by Cohen et al. [40] for fish opercula: 1) submerged in acetone for 24 hours to remove lipids and tissue, 2) heated in an oven (ThermoFisher, Waltham, Massachusetts) for 3 hours at 100° C to re-



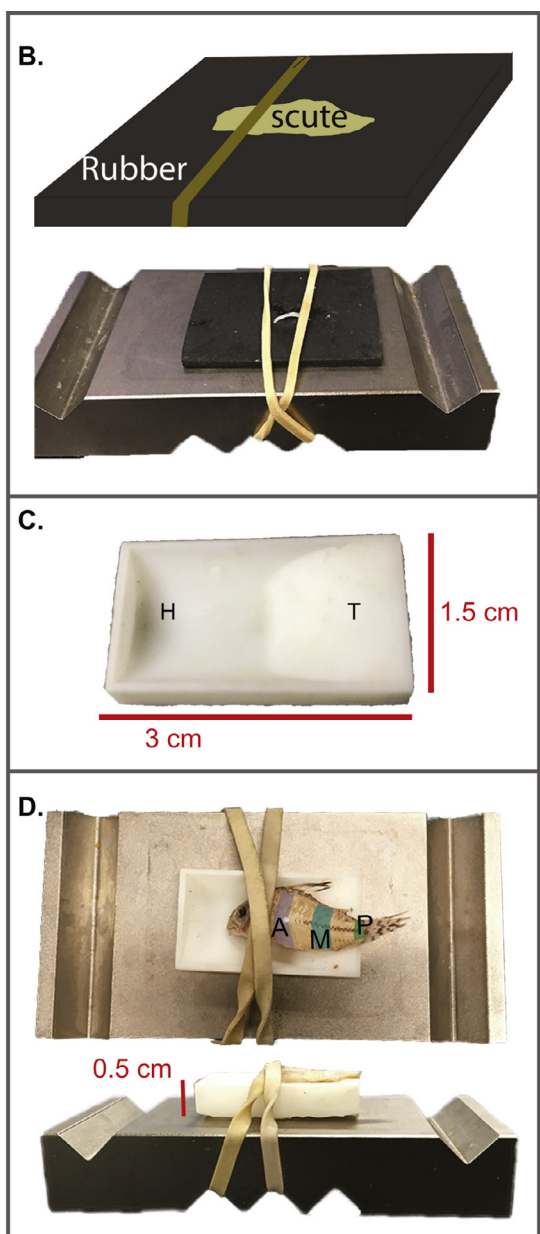


Fig. 1. Experimental set-up for puncture tests. A) Instron materials tester loaded with needle. Punctures are administered in a downward motion. Rubber backing is secured to a metal plate. Scales removed from the fish would be placed on top of the rubber and secured with the rubber band. B) Illustration and photograph of the rubber set-up. C) Fish bed design showing the region that supports the head (H) and the elevated region that supports the tail (T). D) Two views of the whole fish tests in the customized fish bed. Note the fish bed is deeper where the fish head lies so that the entire fish remains in a horizontal position. Colors coded on the fish represent anterior (A), middle (M), and posterior (P) locations for puncture tests. Depth of the fish bed at the head region was 0.5 cm.

move water, 3) weighed to determine dry mass (organic and mineral content), 4) heated for 10 hours at 500° C to burn off organic content, and 5) then weighed the remaining dry ash.

2.3. Imbrication and Overlap

Imbrication (Eq. 1), or the proportion of exposed area, is a common measurement to compare biological armors [11,15,27,41,42]. Imbrication is typically calculated as

$$Imbrication = EL/TL (1)$$

where EL is the exposed length of the scale and TL is the total length of the scale. Conventionally, degree of imbrication calculates the proportion of exposed length, and not the percentage of overlap [42]. However, the scutes of *C. trilineatus* are elongated in the

dorsal-ventral plane compared to typical fish scales [43], and as such, the percentage overlap between adjacent scutes was also reported to better depict the scute-scute interactions. Seven *C. trilineatus* were used for scute overlap calculations. The same regions were used as with bone ash content tests. Scutes were removed from the body using the extraction procedure described above. We used ImageJ on images taken through a dissecting microscope with an iPhone 6s camera (Apple Inc., 12 megapixels) to trace an area of overlap between the two scutes. In this study, the percentage overlap was calculated as (Eq. 2)

% Overlap =
$$100 * \frac{\text{Area of overlap}}{\text{Area of posterior scute}}$$
 (2)

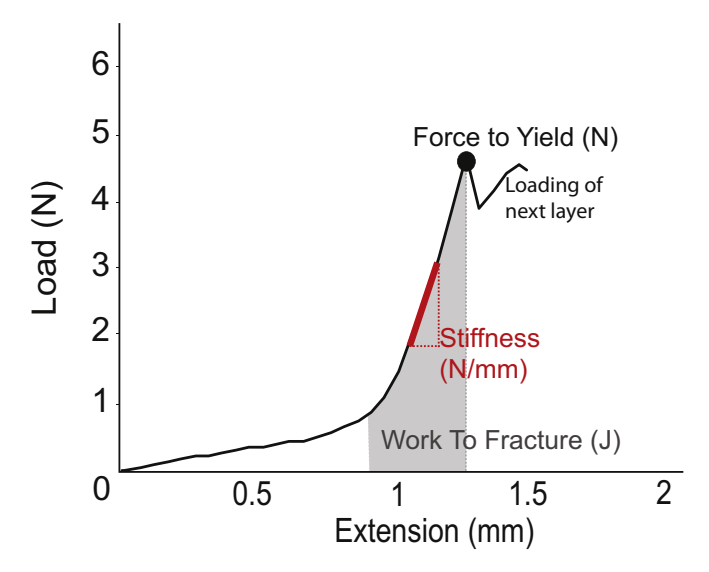


Fig. 2. Example of load-extension curve for puncture tests. Representative data collected from curve are marked to illustrate the force to yield (black dot), stiffness (red line at the linear portion of the curve), and the work to fracture (the area under each curve, marked by the grey shaded region). We chose to conservatively estimate the energy under the curve at the beginning of the linear region as the early portion of the loading resulted in flattening of the scales when compressed by the needle.

2.4. Performance

To examine the mechanical properties of the *C. trilineatus* scutes and armor, we tested three conditions: 1) synergistic effects of multiple overlapping scutes when keeping scutes intact on the body vs. removing scutes - either as a single scute or as a complex comprising multiple scutes, 2) the surface of the scute (external or internal), and 3) the region of the body (anterior, middle, and posterior). Provided the hyaloine is hypermineralized and is located only on the external surface of a scute, then puncturing through the external surface should: 1) require more force, 2) require less energy (more brittle), and 3) result in a stiffer external side compared to the internal.

Fifteen C. trilineatus were used for puncture tests using an 18gauge needle. Fish were euthanized and then scutes were removed from one side of the body (left or right) using the same procedures outlined above. Scutes were either removed individually (single scute puncture test) or together as a complex of two to four overlapping scutes (scute overlap puncture tests). The specimen was then examined under a dissecting microscope (Zeiss SteReo Discovery.V20, Zeiss Microscopy, Jena, Germany) to make sure no scutes remained attached prior to testing. The detached scutes were placed in 1.5 mL microcentrifuge tubes containing water pulled from the aquarium tank housing C. trilineatus prior to puncture tests to ensure the scutes were hydrated, as hydrated scales mechanically perform differently than dehydrated scales. For example, Garrano et al. [44] found that hydrated Cyprinius carpio scales had twice the flexibility and strength as dehydrated scales and Wang et al. [11] found that hydrated pangolin (Manis pentadactyla and M. tricuspis) scales showed significantly less flexibility and tensile strength, but higher tensile strain compared to dehydrated scales. We opted to maintain hydration by immersing the scutes in water taken from the live fish tank rather than using a Ringer's or other such solution. The external scutes were already acclimated to these conditions and therefore would not suffer from physiological effects associated with immersion in a hypertonic or hypotonic solution. Our goal was to reduce the amount of dehydration and/or calcium leaching that occurs when adjusting the composition of the hydrating solution. Scutes remained hydrated from the time of removal up until the moment of testing, within 24 hours of extraction. Testing usually occurred within an hour of removal.

We tested the puncture performance and resistance to puncture in C. trilineatus scutes using an Instron 5942 mechanical testing machine (Instron Corp., Norwich, MA). These tests were chosen to simulate the relevant puncture force the scutes encounter in the wild - the assault of a predator's tooth. We measured the diameter (1.30 mm) of an adult red-bellied piranha (Pygocentrus nattereri) tooth marked at the distal third of its height because that is the approximated penetration distance for a piranha tooth [25,45]. We used an 18-gauge needle to puncture the scutes because its outer diameter (1.27 mm) is roughly equal to the diameter of a P. nattereri tooth. Needles were regularly swapped out throughout the study. While the 18-gauge needles and a P. nattereri tooth are surely different in aspect ratio, the initial damage of the 18-gauge needle should be a useful approximation of the predator. We note that we selected piranha as the model for our puncture performance tests because 1) they are found in similar waters as C. trilineatus, 2) have been reported to show predatory behaviors toward our study organism, and 3) in lab predatory events (per obs.) showed that C. trilineatus can withstand repeated bites (and survive seemingly unharmed) from juvenile P. nattereri.

2.5. Whole body tests

We punctured scutes kept intact along the length of the whole body of the euthanized C. trilineatus (N=11 specimens; average 4.9 punctures (range: 2-6); 54 total punctures were analyzed). Specimens were placed in a 30 mm x 15 mm x 5 mm customized, 3D-printed (Formlabs Form 2 3D Printer, Formlabs Inc., Somerville, MA) "fish bed" designed to hold the specimen in place (Fig. 1). Through trial-and-error, the "fish bed" was designed to match the fish body's natural curvature to prevent dorso-ventral rotation during puncture testing. The head of the fish bed was deep enough to support the entire head of the fish while the bed became increasingly shallower by mimicking the natural curvature of the fish to support the caudal fin; the goal of the design was for the side being punctured to be flat (not laterally bent) during testing (Fig. 1). A rubber band was secured around the fish bed in a dorsal-ventral direction to hold the specimen in place and decrease anteriorposterior movement.

For each region of the fish body (anterior, middle, and posterior), the dorsal and ventral scutes (both intact and detached, and the internal and external surfaces) were punctured (Anterior scutes: N=15 specimens, average 6.8 punctures (range: 2-12), 102 total punctures; Middle scutes: N=15 specimens, average 6.2 punctures (range: 2-10); 93 total punctures; Posterior scutes: N=14 specimens, average 5.6 punctures (range: 2-9), 79 total punctures). The needle and scute(s) were initially aligned to puncture the estimated geometric centroid of the scute(s). A puncture was counted if there was evidence of cracking or denting in the scute (determined via verification through examination under a dissecting microscope). A hole in the scute counted as a full puncture. If the scute was not punctured (no sign of impact as detailed previously), then the trial was reset and aimed at either the same scute (if there was no penetration) or an adjacent scute in the same region (if the previous test resulted in an incomplete puncture). When multiple punctures were performed on the same scute, all of those punctures were averaged to obtain a single data point per scute for analysis, corresponding with the noted puncture totals. The puncture tests were performed at a displacement rate of 0.5 mm s⁻¹ for a distance of 2.0 mm, settings that are slow enough to reduce slippage of the needle on the scutes and deep enough to puncture fully without impacting the underlying body tissue.

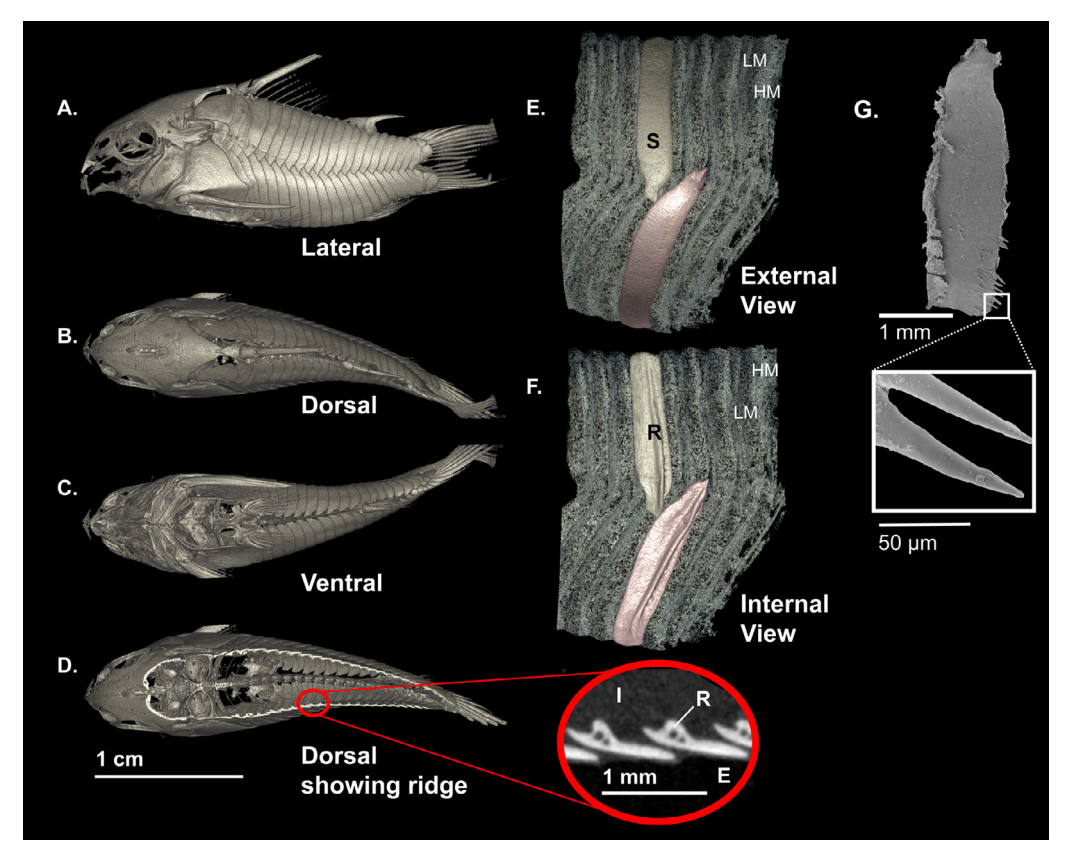


Fig. 3. Anatomy of Corydoras trilineatus scutes. A) Micro CT scan showing the axial scutes in lateral view, B) Dorsal view, and C) Ventral view. D) Dorsal view sectioned to illustrate the intact scute anatomy. The red circle is a closer view of individual scutes illustrating the internal (I) body of the fish, external (E) to the fish, and the deep connective ridge (R). E) Closer view of the external, smooth (S) scute surface and F) the internal scute surface highlighting a medial view of the internal ridge (colored scales). The other scales illustrate relative levels of mineralization where high mineralized areas (HM) correspond to the location of the deep ridge while thinner, less mineralized areas (LM) occur in areas of overlap. G) Scanning electron microscopy of an individual scale. The white box shows a closer view of the odontode (denticles) along the posterior surface of the scute.

2.6. Detached scutes

We punctured either the superficial external surface (N=14 specimens, average 12.2 punctures (range: 3-18), 171 total punctures including intact scutes were analyzed) or the deep internal surface (N = 11 specimens, average 9.4 punctures (range: 7-13), 103 total punctures of only detached scutes were analyzed) of detached C. trilineatus scutes from the three body regions. Single scutes (N=12, average 10.1 punctures (range: 6-14), 121 total punctures) as well as complexes of overlapping scutes (N=13, average 7.6 punctures (range: 1-15), 99 total punctures) from each of the three body regions were used. The needle was aligned to puncture the estimated geometric centroid of the scute, and then additional punctures were performed along the scute to test for consistency; one dorsal and one ventral to the geometric centroid. The punctures were first analyzed as individual tests (each puncture as an independent puncture). The three punctures for each scute were then averaged to obtain a single data point for analysis, corresponding with the noted puncture totals above. A rubber layer with a compressive elastic modulus of ~1 MPa was placed underneath the scute to simulate soft tissue under the scute (Fig. 1), a method established by Meyers et al. [25]. The scutes were placed on the rubber and held in place with a rubber band to reduce torsional rotation. A puncture prior to each scute was performed on the rubber to calibrate the needle and allow for pre-loading the needle with the scutes pressed to the rubber to prevent scutes from moving upon impact. The puncture tests were performed at a displacement rate of 0.5 mm s^{-1} for a distance of 1.5 mm.

Scutes were either punctured through the external surface or the internal bony base, but not through both (the puncture was programmed to only collect data up until the initial break, as that corresponded with the fracture of the target layer (Fig. 2)). Flipping the scute was the most practical method to test scutes without hyaloine, as a review of the scientific and dental literature indicated that there is currently no method developed to remove hyaloine or other hypermineralized tissue from bone and keep it in a solid state suitable for mechanical properties tests [46,47].

2.7. Calculations

The mechanical properties measured were force to yield (Newtons), stiffness (N/mm), and work to fracture (joules). Force to yield was recorded as the force of the yield point (data only collected at the initial break and not for reloading events following) of the load-extension curve (Fig. 2). Stiffness was calculated by dividing the difference in force of two load points along the linear region by the difference in extension of the same two points. The value for stiffness was calculated within the linear region of the load-extension curve prior to yielding (Fig. 2). Work to fracture was calculated as the area under the load-extension curve (see below and Fig. 2) from the end of the toe region (the beginning of the linear region) to the yield point of the load-extension curve (the point of puncture) (Fig. 2; Eq. 3).

Work To Fracture
$$=\int_{a}^{b} F(x) dx$$
 (3)

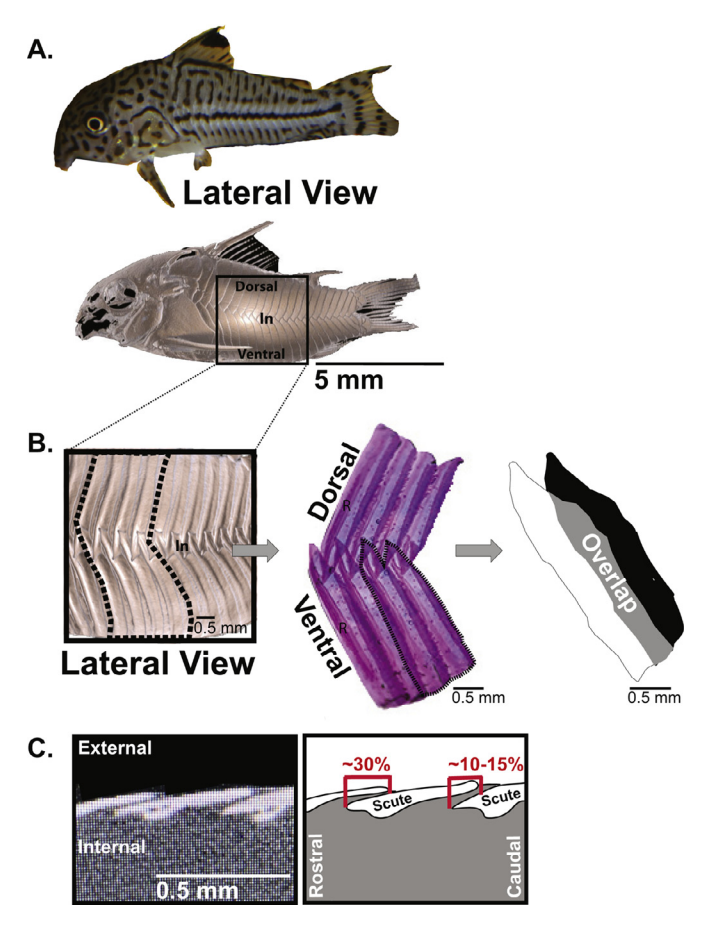


Fig. 4. Scute anatomy and overlap. A) Live *C. trilineatus* showing epithelial covering and a CT scan of fish illustrating the dorsal and ventral rows of scutes as well as the interlocking pattern (In) along the horizontal margin. B) Closer view of the surface scutes and a cleared and stained image of the scutes demonstrating mineralization patterns. Dashed line along the CT scan indicates scutes removed for cleared and stained images. Darker purple indicates areas of higher mineralization. The cartoon (grey) illustrates scale overlap. The anterior scute of the pair is white, the posterior scute is black, and the area of overlap between them is shaded grey. C) Static image from micro CT scan and illustration showing the scute overlap of approximately 30% along the rostral (anterior) scute and 10-15% along the caudal (posterior) scute.

Where b is located at the yield point and a is located at the end of the toe region. The toe region was excluded because there was slight movement of the scute as it "flattened out" while the needle was being applied to the scute.

2.8. Verification of puncture

We used a Scanning Electron Microscopy (SEM) to image 3 punctured scutes. This provided a verification mechanism to closely inspect the scute for crack propagation and surface tissue damage. In addition, this provided a closer view of the anatomical structure of the scutes and the position and shape of the denticles as they are attached on the posterior surface of the scute. Scales were dehydrated gradually over a 48-hour period into 100% ethanol [48]. Specimens were dried using a Quorum E3100 Critical Point Dryer (Quorum Technologies Ltd, East Sussex, UK), sputter coated, and imaged using a Hitachi S-2400 (25 KV) SEM.

2.9. Statistical Methods

We tested the residuals for normality of the data using the Shapiro-Wilk test and for variance using the Fligner-Killeen test. Only the amount of overlap between scutes and the organic composition of the scutes followed a normal distribution and homo-

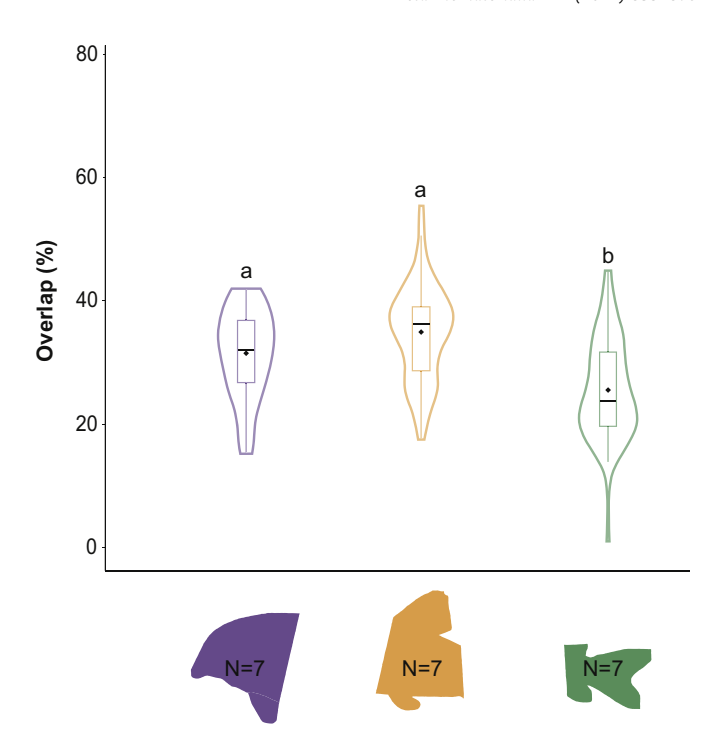


Fig. 5. Scute overlap. Hybrid violin-box plots of percentage of scute overlap grouped by region of the body (N = 7). The width of the curvature of the violin represents the distribution of the data. The upper, middle, and lower bars of the box plots represent the 75% quantile, median, and 25% quantile, respectively. Diamonds represent the mean. The regions of the body are color coded as anterior (purple), middle (orange), and posterior (green). The anterior region average overlap was $33.13\% \pm 1.16$ SE, the middle region averaged $36.19\% \pm 1.00$, and the posterior region averaged 29.22 ± 1.04 . Non-matching letters indicate mean values that differ significantly. The amount of overlap in the posterior region was significantly less than in the anterior (p = 0.039) and middle (p < 0.001) regions.

geneity of variance, even following data transformations. For these two data sets, one-way ANOVAs were run followed by Tukey's post hoc tests [49]. Significance was determined at p-values < 0.05. For all other data, Kruskal-Wallis tests were applied followed by post hoc Nemenyi tests to detect differences in the percent composition (mineral and water), differences in the force to yield, stiffness, and work to fracture among each region of the body, type of scute punctured (single, overlapping detached, and intact), and scute surface punctured [49]. Because multiple punctures were performed per scute and averaged per scute, statistical analysis tests were performed on both the averaged data set and as individual punctures (not averaged). There were no differences in significance between the two data sets. The analysis of the averaged data is shown. All statistical analyses were performed in R versions 3.4.3 – 3.5.2 [50] and figures were produced using the package ggplot2 [51].

3. Results

3.1. Scute Anatomy and Overlapping Scutes

The scutes in *C. trilineatus* run the length of the axial body posterior to the parieto-supraoccipital down to the caudal peduncle (Fig. 3) similar to *C. aeneus* [52]. The two rows of lateral scutes form an alternating interlocking pattern along the horizontal margin of the body (Fig. 3A); however this same interlocking pattern is not present on the dorsal and ventral surfaces of the body (Figs. 3B & 3C, respectively). The internal surface of the scute has an underlying, thickened ridge that anchors the scute to the underlying soft tissue (Fig. 3D), while the external surface of the scute appears smooth and flat (Fig. 3E). The ridge position corresponds to areas with little to no scute overlap (Figs. 3F & 3G). This results

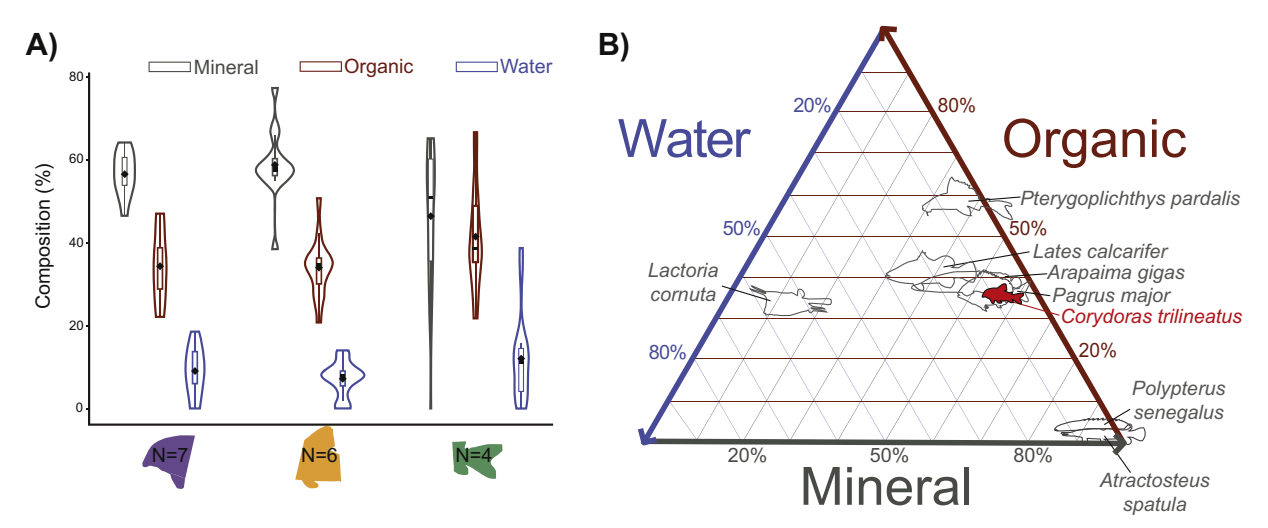


Fig. 6. A) Hybrid violin-box plots of average percentage of mineral (gray, $53.62\% \pm 1.63$ SE), organic (brown, $36.86\% \pm 1.63$), and water (blue, $9.53\% \pm 1.63$) composition of the *Corydoras trilineatus* scutes (N = 7) grouped by region of the body. The width of the curvature of the violin represents the distribution of the data. The upper, middle, and lower bars of the box plots represent the 75% quantile, median, and 25% quantile, respectively. Diamonds represent the mean. The regions of the body are divided into anterior (purple), middle (orange), and posterior (green). Non-matching letters indicate values that differ significantly and no letters indicates there is no significant difference among regions for each type of composition. There were no significant differences between the regions for each type of composition (p = 0.156 for mineralization, p = 0.068 for organic, and p = 0.348 for water). B) Ternary diagram of the percent compositions of various armored fishes (outlined shapes). Relative proportions were determined by mass. Comparative data are from various sources [13,15,22,26,53-55].

in thinner areas that are reinforced structurally with overlap and thicker in areas with no overlap. The scutes are covered with a thin layer of epithelium (Fig. 4A) that provides distinctive color patterns along the length of the fish. Closer examination using CT technology reveals the interlocking mechanism described above is more prominent toward the rostral portion of the axial skeleton (Figs. 4B and 4C).

Corydoras trilineatus scutes averaged (\pm SE) 32.71% \pm 0.77 (N = 7) overlap (Figs. 4B and 4C; Fig. 5). The posterior scutes overlapped significantly less (29.22% \pm 1.04) than both the anterior (33.13% \pm 1.16, p = 0.039) and middle scutes (36.19% \pm 1.00, p < 0.001), but there was no significant difference between the anterior and middle scutes (p = 0.141). Cleared and stained images and CT images of scute overlap reveal that there are approximately equal amounts of overlap along the rostral and caudal surfaces of the scutes, although these ratios change somewhat along the length of the body (Figs. 4B and 4C).

3.2. Composition

The scutes of *C. trilineatus* were highly mineralized, with an average (\pm SE) mineral composition of approximately 53.62% \pm 1.63 (N = 7) (Figs. 4B, 6). The organic and water compositions averaged 36.86% \pm 1.63 and 9.53% \pm 1.63 (N = 7), respectively (Fig. 6). However, there were no significant differences among the regions of the body for mineralization, organic, or water composition, respectively (p = 0.156 for mineralization, p = 0.068 for organic, and p = 0.348 for water).

3.3. Scanning Electron Microscopy

Scanning electron microscopy confirmed punctures in selected scutes. Evaluations of crack propagation throughout the surrounding scute showed that cracks did not visually propagate farther than 10 μ m from the puncture site (Fig. 7).

3.4. Scute performance

Intact scutes had significantly lower average (\pm SE) forces to yield (1.55 \pm 0.09 N; N = 11) than both detached overlapping (1.88

 \pm 0.07 N, N = 12, p = 0.025) and detached single scutes (2.02 \pm 0.06 N, N = 13, p < 0.001) (Figs. 8A and 8B). However, deep punctures of intact scutes were rarely observed. Instead, most of the punctures of intact scutes were shallow and/or caused only cracks or dents. The scutes kept intact on the body had significantly lower stiffness (2.54 \pm 0.25 N/mm) than both of the detached scute groups (7.28 \pm 0.19 N/mm for overlapping and 7.99 \pm 0.17 N/mm for single, p < 0.001 for both) (Figs. 8A and 8C). There were significant differences in work to fracture among the different scute groups; intact scutes required the most energy (0.66 \pm 0.05 J, p = 0.005 to single detached, p < 0.001 to overlapping) to fracture, with single detached scutes (0.42 \pm 0.03 J, p = 0.015 to overlapping) next, followed by overlapping detached scutes (0.31 \pm 0.03 J) (Figs. 8A and 8D).

3.5. Body region

When puncturing with the needle, posterior scutes had a significantly lower average (\pm SE) force to yield (1.69 \pm 0.08 N) than scutes from the middle region (1.94 \pm 0.07 N) (p = 0.045), with no significant differences between either of those regions and the anterior region (1.97 \pm 0.07 N) (Figs. 9A and 9B). There were no significant differences in stiffness among the regions of the body (p = 0.099) (Figs. 9A and 9C). There were no significant differences among the regions of the body in terms of energy required to puncture (p = 0.653) (Figs. 9A and 9D).

3.6. Surface performance

When puncturing the scute(s) with the needle, the force to yield did not differ significantly between the external and internal surface of the scutes (p = 0.121) (Figs. 10A and 10B). The internal surface of the scutes (8.52 \pm 0.23 N/mm) were significantly stiffer than the external surface (5.53 \pm 0.18 N/mm) (p < 0.001) (Fig. 10C). There was no significant difference in the work to fracture of the two surfaces of the scute (p = 0.623) (Fig. 10D).

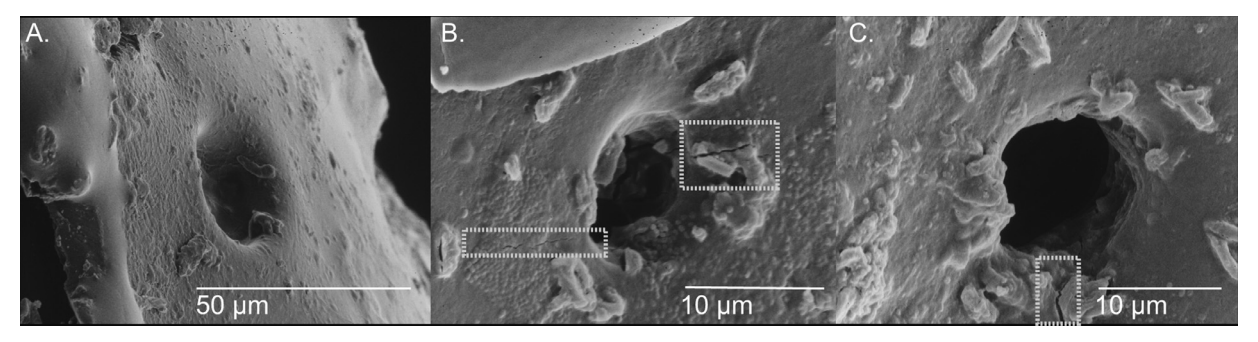


Fig. 7. Scanning electron images of *C. trilineatus* scutes from intact (whole fish) puncture tests. A) Puncture from needle with no visible microdamage to surrounding scute. B-C) Representative punctures showing crack propagation (grey dashed boxes) in surrounding tissue. Cracks that did occur were located within 10 microns from the puncture site.

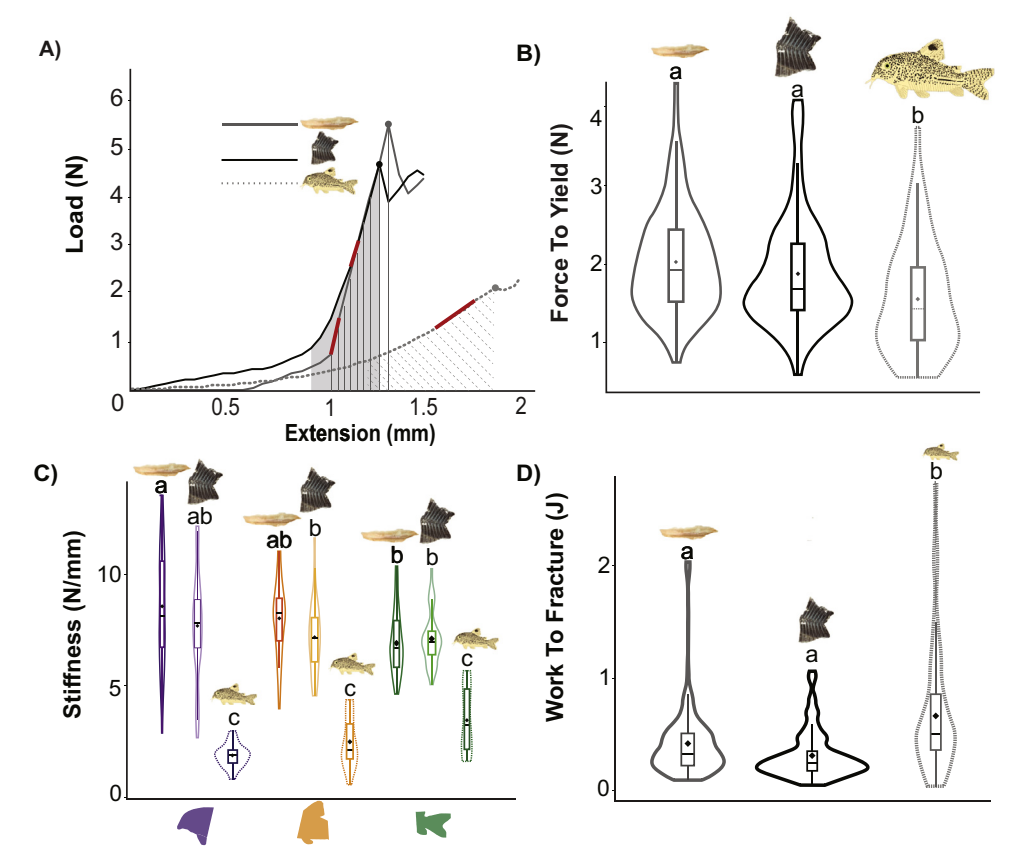


Fig. 8. A) Mechanical tests for scutes intact and removed from the body. Examples of load-extension curves for each region of the body that was punctured with markings corresponding to the force to yield (colored dot), stiffness (red line at the linear portion of the curve), and the work to fracture (the area under each curve, marked by the grey shaded region and corresponding colored lines). B-D) Hybrid violin-box plots of the force to yield, stiffness, and work to fracture calculated from puncturing tests of *Corydoras trilineatus* scutes (N = 15) grouped by type of scute(s) punctured (single detached scute, multiple overlapping detached scutes, and scutes intact on the fish body), measured in Newtons, N/mm, and joules, respectively. The width of the curvature of the violin represents the distribution of the data. The upper, middle, and lower bars represent the 75% quantile, median, and 25% quantile, respectively. Diamonds represent the mean. Non-matching letters indicate mean values that differ significantly. The regions of the body in C) are color coded as anterior (purple), middle (orange), and posterior (green). The intact scutes had significantly lower strength than both detached scute groups (p = 0.025 to overlapping and p < 0.001 to single; B), were significantly less stiff than both other groups along the entire body (p < 0.001; C), and needed significantly more energy to puncture than both other groups (p = 0.005 to single detached and p < 0.001 to overlapping; D).

4. Discussion

The shape and length of *Corydoras* sp. scutes differ greatly from other more commonly examined fish scales. For example, *Corydoras* scutes cover approximately 46% of the body depth (measured using ImageJ) compared to the 1-5% of body depth reported for other notable fish scales - e.g. large-scale loach (*Paramisgurnus dabryanus*), piracuru (*A. gigas*), and goldfish (*Carassius auratus*) [43]. *Corydoras* scutes overlap less (~33%) than the scales of

other fishes like *A. gigas* (>60%) [3], coelacanth (L. chalumnae) (66%) [15], amazon sailfin catfish (*Pterygoplichthys pardalis*) (50%) [32], striped bass (*M. saxatilis*) (50%) [55], mullet (Mugilidae sp.) (70%) [55], and milkfish (*Chanos chanos*) (80%) [55]. The overlap more closely matches the level of overlap seen in fishes with more specialized protective coverings like alligator gars (*A. spatula*) (22-30%) [27] and boxfish (*Lactoria cornuta*) (0%) [56] and terrestrial animals like Chinese pangolins (*M. pentadactyla*) (29%) and African pangolins (*M. tricuspis*) (43%) [11]. The low percentage of overlap

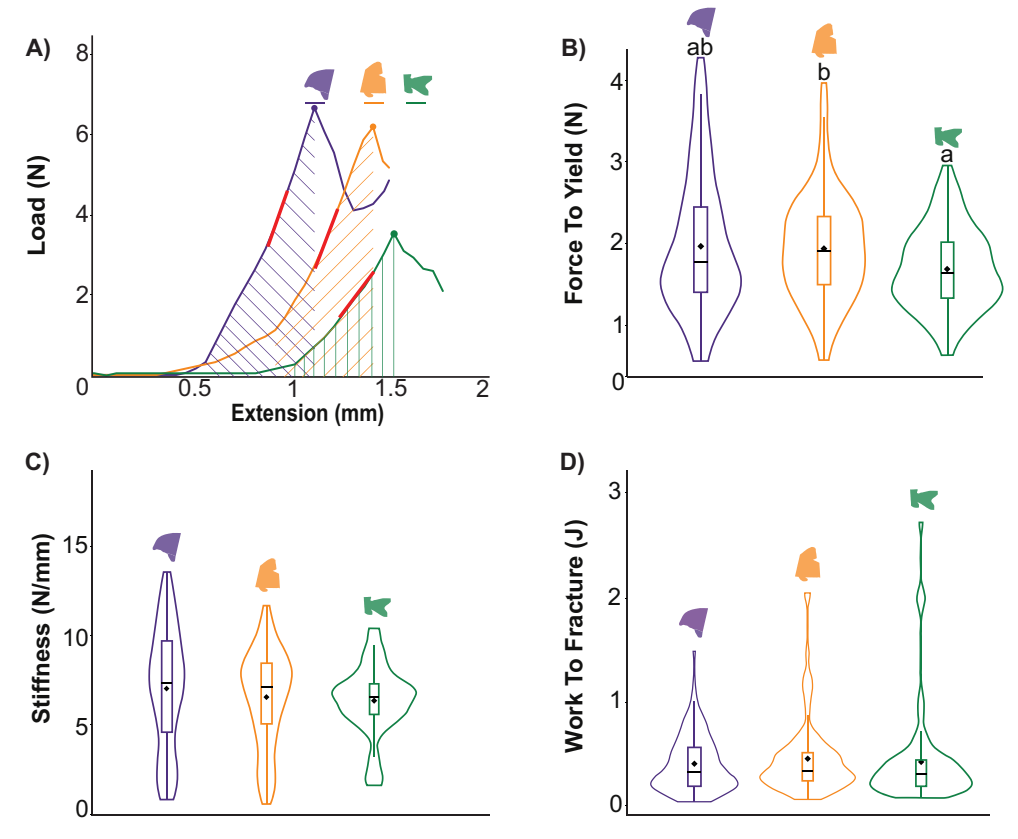


Fig. 9. A) Mechanical tests for region of the body: anterior, middle, posterior scutes. Examples of load-extension curves for each region of the body that was punctured with markings corresponding to the force to yield (colored dot), stiffness (red line at the linear portion of the curve), and the work to fracture (the area under each curve, marked by the corresponding colored lines). B-D) Hybrid violin-box plots of the force to yield, stiffness, and work to fracture calculated from puncturing tests of *Corydoras trilineatus* scutes (N = 15) grouped by region of the body, measured in Newtons, N/mm, and joules, respectively. The regions of the body are color coded as anterior (purple), middle (orange), and posterior (green). The width of the curvature of the violin represents the distribution of the data. The upper, middle, and lower bars of the box plots represent the 75% quantile, median, and 25% quantile, respectively. Diamonds represent the mean. Non-matching letters indicate mean values that differ significantly and no letters indicates there is no significant difference among groups. Scutes from the posterior region had a significantly lower strength than the middle scutes (p = 0.045, B), despite showing no difference in stiffness (p = 0.099; C) or work to fracture among the three regions (p = 0.653; D).

is on par with other inflexible armors, as other fish with similar or less overlap are often described as having "rigid" scales.

In fishes, it is no surprise that larger fish can withstand more puncture force. It is important to note that the size and shape of an indenter directly affects the force to puncture; nevertheless, there are some interesting trends that emerge when correcting for size differences. We note, for this comparison we are using the size and weight of the animals tested if published, or if unavailable, we used a conservative estimate for size (CS) and weight (CW). Arapaima gigas can withstand up to 150 N when puncturing a detached scale using a piranha tooth, and in fact, no tooth fully punctured the scales and some piranha teeth broke during the puncture trials [25,57]. Similarly, A. spatula withstands up to 500 N when punctured by an alligator tooth, which also broke before fully puncturing intact scales; [15]. However, both A. gigas (~200 cm SL; 90 kg CW) and A. spatula (~200 cm SL; 70 kg CW) are two orders of magnitude longer and at least four orders of magnitude more massive than the C. trilineatus in this study (2.5 cm SL; 0.001 kg). Yet the force to puncture these large-scaled fishes did not scale with mass; instead they differed by just two orders of magnitude. The comparison to other smaller armored fishes is more extreme. Latimeria chalumnae scales (160 cm CS; 81 kg CW) withstood up to 25 N when subjected to puncture tests on two overlapping, detached scales using a shark tooth [15]. Additional examples include striped bass (M. saxatilis) (~60 cm TL (CS); 31 kg CW) that withstood up to 14 N when puncturing intact scales; [26] and boxfish (Lactoria cornuta) (46 cm TL; 0.1 kg CW) that withstood up to 85 N [56]. In comparison to *C. trilineatus*, these other fishes withstood just one order of magnitude more force before succumbing to puncture though they were between two to four orders of magnitude more massive.

Previous studies on fish armors have shown that multiple overlapping scales require more energy to puncture than individual scales and the force of puncture through multiple scales is three to five times higher than puncturing through isolated individual scales/scutes [26,55]. Our study followed a similar trend with multiple scutes requiring approximately 20-30% more force than puncturing through an individual scute. However, C. trilineatus scute placement revealed there is approximately 40% overlap in scutes at the anterior and posterior edges of a scute, though the middle of the scute does not have reinforcement from overlapping scutes. Instead it is equipped with a highly mineralized internal ridge that helps to reinforce the scutes. In addition to structural reinforcement via overlapping scutes, C. trilineatus makes use of hard to soft interfaces to structurally reinforce the scutes. Puncturing the external surface of the scute requires penetration through two distinct layers, the hypermineralized hyaloine and type I collagen - hard and soft materials, respectively, while directly puncturing the internal surface of the scute requires penetration of only the internal layer of lamellar bone - hard material only. The external surface of the C. trilineatus scute required significantly more work to puncture than the underlying internal surface that is attached to the body. Puncturing the C. trilineatus armor with the scutes intact on the body required approximately 50-100% more energy to fracture

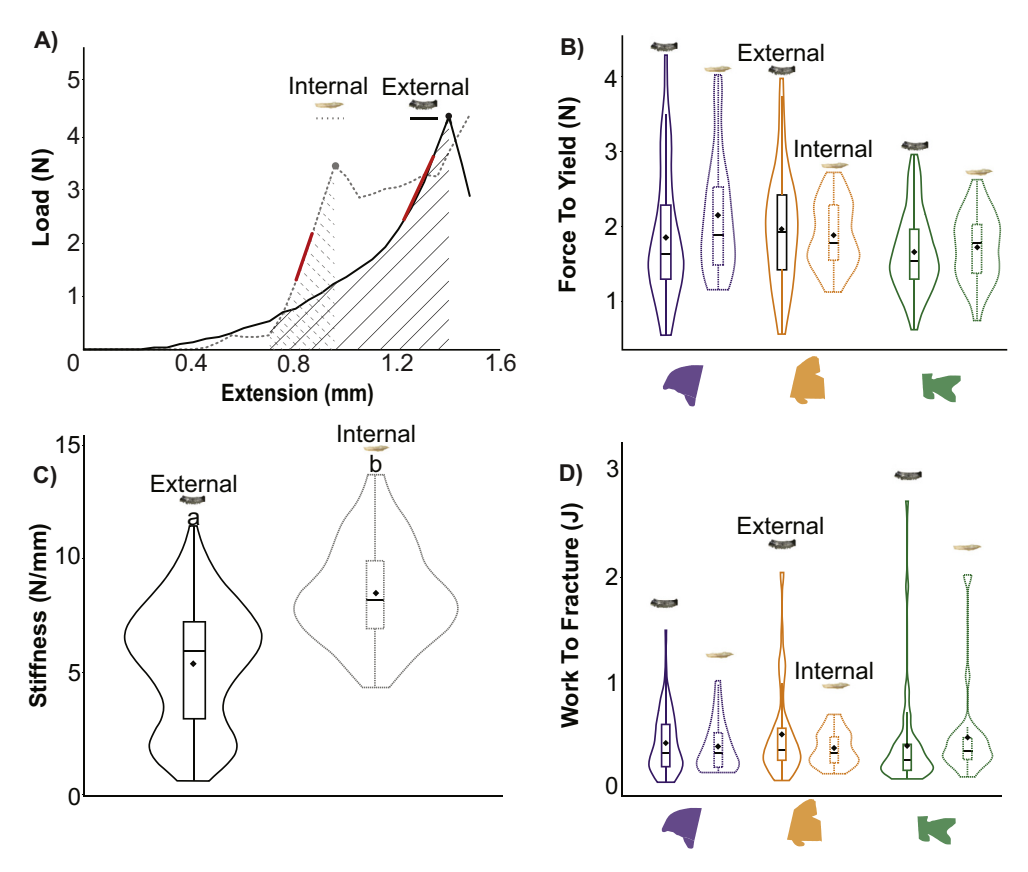


Fig. 10. Mechanical tests for internal and external surface of the scutes. A) Examples of load-extension curves for each region of the body that was punctured with markings corresponding to the force to yield (colored dot), stiffness (red line at the linear part of the curve), and the work to fracture (the area under each curve, marked by the corresponding patterned lines). B-D) Hybrid violin-box plots of the force to yield, stiffness, and work to fracture calculated from puncturing tests of *Corydoras trilineatus* scutes (N = 15) grouped by region of the body and surface of the scute punctured (external or internal, measured in Newtons, N/mm, and joules, respectively. The regions of the body are color coded as anterior (purple), middle (orange), and posterior (green). The width of the curvature of the violin represents the distribution of the data. The upper, middle, and lower bars of the box plots represent the 75% quantile, median, and 25% quantile, respectively. Diamonds represent the mean. Non-matching letters indicate mean values that differ significantly and no letters indicates there is no significant difference among groups. The internal surface of the scutes had significantly higher stiffness than the external surface (p < 0.001, C)

than puncturing the scutes detached from the body, thus confirming that intact armor is tougher than detached scutes. *Corydoras* are certainly not novel in their use of hard to soft reinforcement. Zhu et al. [26] showed that fish scales are stiffer than the body tissue substrate, which results in the scales "sinking" into the tissue upon compression. During a predation event, this "scale sinking" may result in an injury to the fish, but it likely prevents fatal puncture. The body may act as a cushion that allows the scale to sink into the underlying dermis upon impact, effectively absorbing the force being applied to the scale, and preventing a destructive puncture. During our post-test, microscopic examination of scutes, we noted that it was rare for puncture tests on intact scutes to puncture through the entire scute.

Corydoras trilineatus scutes are highly mineralized (53%) relative to other armored fishes (16-59%), a group that includes piracuru (A.~gigas) (internal layer = 39%, external = 58%) [15,58], red seabream (Pagrus~major) (whole scale average 46%) [13], striped bass (M.~saxatilis) (internal = 14%, external = 50%) [26], and a larger Amazonian armored catfish (P.~pardalis) (internal = 44%, external = 50%) [58]. Unfortunately, we were unable to reliably separate the internal and external layers of the scutes for direct comparison due to their small size and the composition of hyaloine. Nevertheless, the relatively high mineral content suggests that the scutes are hard (resistant to plastic deformation), but also brittle (breaks with little plastic deformation) similar to other highly mineralized biological materials (e.g. enamel mineralization = 97% mineralization; Dentine = 70%) [59]. However, al-

though the scutes do succumb to punctures, the scutes are reinforced so that crack propagation does not compromise the entire structure. Brittle scutes would not likely withstand repeated high force attacks. However, the scute is a composite material. Toughening the hyaloine by embedding it in a more ductile material (connective tissues, etc.) results in the scute performing as a stronger structure than either of the materials would perform on their own. It is therefore not surprising that they are reinforced by a cushioning effect via connective fibers throughout the scute and in conjunction with the underlying soft tissues. Other examples of this synergism are found throughout the natural world. Biological tissues tend to become stiffer as they become more mineralized; mineralization usually couples with calcification in vertebrates [59-61]. Highly mineralized biological tissues (ex. teeth in mammals composed of enamel, dentine, and tooth cement) avoid structural failure via deformation (brittleness) by 1) making use of areas of high and low mineralization within the tooth and 2) arranging fibers and mineralized layers to reduce crack propagation [59]. We noted in the SEM images that crack propagation expanded just 10 µm from the puncture site. Although we cannot say with absolute certainty that there was no further compromise to the scute following a penetrative event, we do note that additional puncture tests on the same scute were comparable in the force to puncture. We therefore argue that the entire scute is not likely to fail following a single predatory bite. We hypothesize that these scutes are arranged to provide the greatest puncture resistance during a single, targeted attack. It is of note that in this study we did not test the performance of replacement scutes.

Biological armors follow a similar composition across taxa, and the small variations in the armors allow them to function as more than just protection from predators [4-7, 11]. The dermal structures that form the armor can be multifunctional, including contributing to a higher locomotive efficiency by reducing drag in fishes to help offset the increase in mass and cost to swim caused by the presence of armor [62,63], providing luminescence in fishes [63], and providing camouflage in chameleons [64]. But armor comes at a cost, both energetically and functionally [14,65]. Biological armor in plantigrade mammals, those that walk on the soles of their feet with the toes and metatarsals flat on the ground, was associated with a lower metabolic rate, slower running speeds, and issues with thermoregulation for smaller species [65]. Animals at higher trophic levels tend to have reduced or no armor because it inhibits speed; however, this tradeoff results in reduced protection against their own predators. Animal armors must contend with this tradeoff between strength, flexibility, and the weight of the armor [14]. Thick, bulky armors like turtle shells provide protection from attacks, but are heavy and limit maneuverability and flexibility. Lighter armors, like fish scales near the tail, allow for wide ranges of motion but do not provide as much protection as stronger scales elsewhere on the body [44]. Even though C. trilineatus is not a particularly fast or flexible swimmer, it does appear that it is flexible enough to fit into small spaces and escape predators. It is unclear whether Corydoras sp. armors serve additional purposes beyond predator protection. We suggest that additional studies further explore the anatomy and scale function across this group of tiny armored fishes.

This study describes the puncture resistance and composition of scutes in a small armored catfish, *Corydoras trilineatus*, and is one of only a few studies that focus on the scute anatomy in the genus *Corydoras*. The armored scutes are highly mineralized; however, the fish retains flexibility of its body. Like with most fish armors, *C. trilineatus* armor is difficult to puncture and the fish uses multiple tricks to reduce puncture including: 1) hard to soft interfaces that increases the puncture resistance and still allows for some flexible mobility, 2) overlap of scutes along the anterior and posterior scute, 3) a reinforced mineralized central ridge that stabilizes the middle portion of the scute where there is no scute overlap, and 4) a composite material to reduce structural failure following a successful puncture.

Declaration of Competing Interest

The authors declare that they have no known competing financial interests or personal relationships that could have appeared to influence the work reported in this paper.

Acknowledgments

This research was supported with funding provided by NSF IOS-1932757 and DBI-1759637. Additional funding was generously provided by the CSUF Hillman McClanahan Scholarship awarded to A.L. and the CSUF Natural Science and Mathematics Interclub Council (NSM-ICC). Thank you to Tammy Lu for providing SEM images of scutes. Micro computed tomography scanning was provided by the Karel F. Liem Imaging Center at the University of Washington Friday Harbor Laboratories. We thank our laboratory volunteers: Megan Nguyen, Kaycee Coonen, and Lindsay Maldonado who assisted with fish husbandry and experimental set ups. Finally, we would like to thank Dr. Kathryn Dickson and four anonymous reviewers for providing extensive and helpful comments that greatly improved this manuscript. All work was conducted in ac-

cordance with protocol 17-R-03 CSUF Institutional Animal Care and Use Committee protocol number 17-R-03.

REFERENCES

- S. Giles, M. Rücklin, P.C.J. Donoghue, Histology of "Placoderm" dermal skeletons: implications for the nature of ancestral gnathostome, J, Morphol 274 (2013) 627–644.
- [2] W. Yang, I.H. Chen, J. McKittrick, M.A. Meyers, Flexible dermal armor in nature, IOM 64 (2012) 475–485.
- [3] W. Yang, I.H. Chen, B. Gludovatz, E.A. Zimmermann, R.O. Ritchie, M.A. Meyers, Natural flexible dermal armor, Adv. Mater. 25 (2013) 31–48.
- [4] T.M. Scheyer, P.M. Sander, Histology of ankylosaur osteoderms: implications for systematics and function, J. Vertebr. Paléontol. 24 (2004) 874–893.
- [5] R.P. Main, A. de Ricqlés, J.R. Horner, K. Padian, The evolution and function of Thyreophoran dinosaur scutes: implications for plate function in Stegosaurus, Paleobiology 31 (2005) 291–314.
- [6] M.R. Seidel, The osteoderms of the American Alligator and their functional significance, Herpetol 35 (1979) 375-38.
- [7] B. Achrai, H.D. Wagner, Micro-structure and mechanical properties of the turtle carapace as a biological composite shield, Acta Biomater (2013) 5890–5902.
- [8] M.K. Vickaryous, B.K. Hall, Osteoderm morphology and development in the nine-banded armadillo, *Dasypus novemcinctus* (Mammalia, Xenarthra, Cingulata), J. Morphol 267 (2006) 1273–1283.
- [9] I.H. Chen, J.H. Kiang, V. Correa, M.I. Lopez, P.Y. Chen, J. McKittrick, M.A. Meyers, Armadillo armor: mechanical testing and micro-structural evaluation, J. Mech. Behav. Biomed. Mater. 4 (2011) 713–722.
- [10] M.K. Vickaryous, J. Sire, The integumentary skeleton of tetrapods: origin, evolution, and development, J. Anat 214 (2009) 441–464.
- [11] B. Wang, W. Yang, V.R. Sherman, M.A. Meyers, Pangolin armor: overlapping, structure, and mechanical properties of the keratinous scales, Acta Biomater 41 (2016) 60–74.
- [12] Y. Bouligand, Twisted fibrous arrangements in biological materials and cholesteric mesophases, Tissue and Cell 4 (1972) 189–217.
- [13] T. Ikoma, H. Kobayashi, J. Tanaka, D. Walsh, S. Mann, Microstructure, mechanical, and biomimetic properties of fish scales from *Pagrus major*, J. Structur. Biol. 142 (2003) 327–333.
- [14] P.Y. Chen, J. McKittrick, M.A. Meyers, Biological materials: Functional adaptations and bioinspired designs. Prog. Mater. Sci. 57 (2012) 1492–1704.
- [15] V. Sherman, H. Quan, R. Ritchie, M. Meyers, A comparative study of piscine defense: the scales of Arapaima gigas, Latimeria chalumnae and Atractosteus spatula, J. Mech. Behav. Biomed. Mat 73 (2016) 1–16.
- [16] E.A. Zimmermann, B. Gludovatz, E. Schaible, N.K.N. Dave, W. Yang, M.A. Meyers, R.O. Ritchie, Mechanical adaptability of the Bouligand-type structure in natural dermal armour, Nat. Commun (2013), doi:10.1038/ncomms3634.
- [17] A.K. Dastjerdi, F. Barthelat, Teleost fish scales amongst the toughest collagenous materials, J. Mech. Behav. Biomed. Mater. 52 (2015) 95–107.
- [18] J.Y. Sire, P.C.J. Donoghue, M.K. Vickaryous, Origin and evolution of the integumentary skeleton in non-tetrapod vertebrates, J. Anat 214 (2009) 409–440.
 [19] M. Bouilliart, M. Paig-Tran, S. Crofts, S. Farina, A. Summers, The post-
- [19] M. Bouilliart, M. Paig-Iran, S. Crotts, S. Farina, A. Summers, The post-cranial body armor of the armored Agonidae fishes-How far do the morphological scale modifications go?, (2014) https://digital.lib.washington.edu/researchworks/bitstream/handle/1773/34614/bouilliart_2014.pdf?sequence=1
- [20] G.H. Roux, The microscopic anatomy of the *Latimeria* scale, S. Afr. J. Med. Sci. 7 (1942) 1–18.
- [21] M.M. Smith, M.H. Hobdell, W.A. Miller, The structure of the scales of *Latimeria chalumnae*, J. Zoöl 167 (1972) 501–509.
- [22] A. Kemp, Formation and structure of scales in the Australian lungfish, Neoceratodus forsteri, (Osteichthyes: Dipnoi), J. Morphol 273 (2012) 530–540.
- [23] B.J.F. Bruet, J.H. Song, M.C. Boyce, C. Ortiz, Materials design principles of ancient fish armour, Nat. Mater 7 (2008) 748–756.
- [24] J.H. Song, C. Ortiz, M.C. Boyce, Threat-protection mechanics of an armored fish, J. Mech. Behav. Biomed. Mater. 4 (2011) 699–712.
- [25] M.A. Meyers, Y.S. Lin, E.A. Olevsky, P.Y. Chen, Battle in the Amazon: Arapaima versus piranha, Adv. Eng. Mater. 14 (2012) B279–B288.
- [26] D.J. Zhu, L. Szewciw, F. Vernerey, F. Barthelat, Puncture resistance of the scaled skin from striped bass: collective mechanisms and inspiration for new flexible armor designs, J. Mech. Behav. Biomed. Mater. 24 (2013) 30–40.
- [27] W. Yang, B. Gludovatz, E.A. Zimmermann, H.A. Bale, R.O. Ritchie, M.A. Meyers, Structure and fracture resistance of alligator gar (*Atractosteus spatula*) armored fish scales, Acta Biomater 9 (2013) 5876–5889.
- [28] M.A. Kolmann, T. Piexoto, J.A. Pfeiffenberger, A.P. Summers, C.M. Donatelli, Swimming and defence: competing needs across ontogeny in armoured fishes, J. R. Soc. 17 (2020) 20200301, doi:10.1098/rsif.2020.0301.
- [29] D.J. Zhu, C.F. Ortega, R. Motamedi, L. Szewciw, F. Vernerey, F. Barthelat, Structure and mechanical performance of a "modern" fish scale, Adv. Eng. Mater 14 (2012) B185–B194.
- [30] W. Meyer, U. Seegers, Basics of skin structure and function in elasmobranchs: a review, J. Fish Biol 80 (2012) 1940–1967.
- [31] J.Y. Sire, Scales in young *Polypterus senegalus* are elasmoid: new phylogenetic implications, Am. J. of Anat. 186 (1989) 315–323.
- [32] D. Ebenstein, C. Calderon, O.P. Troncoso, F.G. Torres, Characterization of dermal plates from armored catfish *Pterygoplichthys pardalis* reveals sandwich-like nanocomposite structure, J. Mech. Behav. Biomedi. Mater. 45 (2015) 175–182.
- [33] W.E. Burgess, An atlas of freshwater and marine catfishes, T.F.H. Publications, Neptune City, 1989.

- [34] S.M. Luna, N. Bailly, Corydoras trilineatus. Retrieved from https://www.fishbase. se/summary/12199. Last accessed September 15, 2019.
- [35] Aquatic Arts, Threestripe Cory: Corydoras trilineatus. Retrieved from https: //aquaticarts.com/products/threestripe-acory-catfish-corydoras-locally-bred. Last accessed October 7, 2020.
- [36] J.Y. Sire, Development and fine-structure of the bony scutes in *Corydoras arcuatus* (Siluriformes, Callichthyidae), J. Morphol. 215 (1993) 225–244.
- [37] J.Y. Sire, A. Huysseune, Structure and development of the odontodes in an armoured catfish, *Corydoras aeneus* (Siluriformes, Callichthyidae), Acta Zoöl 77 (1996) 51–72
- [38] R.J. Riley, E.R. Gillie, A. Jungwirth, J. Savage, N.J. Boogert, A. Manica, The role of tactile interactions in flight responses in the bronze cory catfish (*Corydoras aeneus*), Ethology 125 (11) (2019), doi:10.1111/eth.12935.
- [39] L.F.C. Tencatt, W.M. Ohara, Two new species of Corydoras Lacépéde, 1803 (Siluriformes: Callichthyidae) from the Rio Madeira basin, Brazil, Neotrop. Ichthyol. 14 (1) (2016) Maringá, doi:10.1590/1982-0224-20150063.
- [40] L. Cohen, M. Dean, A. Shipov, A. Atkins, E. Monsonego-Oman, R. Shahar, Comparison of structural, architectural and mechanical aspects of cellular and acellular bone in two teleost fish, J. Exp. Biol. 215 (2012) 1983–1993.
- [41] A. Browning, C. Ortiz, M.C. Boyce, Mechanics of composite elasmoid fish scale assemblies and their bioinspired analogues, J. Mech. Behav. Biomed. Mater. 19 (2013) 75–86.
- [42] W. Yang, V.R. Sherman, B. Gludovatz, M. Mackey, E.A. Zimmermann, E.H. Chang, E. Schaible, Z. Qin, M.J. Buehler, R.O. Ritchie, M.A. Meyers, Protective role of *Arapaima gigas* fish scales: structure and mechanical behavior, Acta Biomater 10 (2014) 3599–3614.
- [43] M. Yu, H. Liu, J. Liu, S. Li, Unique structure and mechanical property of Dabryanus scale, J. Bionic Eng. 13 (2016) 641–649.
- [44] A.M.C. Garrano, G. La Rosa, D. Zhang, L.-N. Niu, F.R. Tay, H. Majd, D. Arola, On the mechanical behavior of scales from *Cyprinus carpio*, J. Mech. Behav. Biomed. Mater. 7 (2012) 17–29.
- [45] J.R. Grubich, S. Huskey, S. Crofts, G. Orti, J. Porto, Mega-bites: extreme jaw forces of living and extinct piranhas (Serrasalmidae), Nat. Scient. Rep 2 (2012) 9.
- [46] R.E.S. Prout, E.R. Shutt, Separation of enamel and dentine using cadmium tungstoborate solution, Arch. Oral Biol 15 (1970) 559–561.
- [47] B.R. Smith, C. Youngberg, D. Finton, D. Willey, T.R. Williams, J.B. Van Doren, A new procedure for separation of the enamel and dentin of human teeth, Talanta 31 (1984) 955–958.
- [48] G.L. Humason, Animal tissue techniques, W.H. Freeman and Company, San Francisco (and London), 1962.
- [49] J.H. Zar, Biostatistical analysis, 5th Edition, Pearson, New York City, 2010.
- [50] R Core Team (2018-2019) R: A language and environment for statistical computing. R Foundation for Statistical Computing, Vienna, Austria. URL http://www.R-project.org/.
- [51] H. Wickham, ggplot2: Elegant graphics for data analysis, Springer-Verlag, New
- [52] F. Huysenstruyt, D. Adriaens, Descriptive osteology of Corydoras aeneus, Cybium 29 (3) (2005) 261–273.

- [53] S. Sankar, S. Sekar, R. Mohan, S. Rani, J. Sundaraseelan, T.P. Sastry, Preparation and partial characterization of collagen sheet from fish (*Lates calcarifer*) scales, Int. I. Biol. Macromol. 42 (2008) 6–9.
- [54] F.G. Torres, O.P. Troncoso, J. Nakamatsu, C.J. Grande, C.M. Gómez, Characterization of the nanocomposite laminate structure occurring fish scales from *Arapaima gigas*, Mater. Sci. Eng. 28 (2008) 1276–1283.
 [55] F.J. Vernerey, F. Barthelat, Skin and scales of teleost fish: Simple structure
- [55] F.J. Vernerey, F. Barthelat, Skin and scales of teleost fish: Simple structure but high performance and multiple functions, J. Mech. Phys. Solids 68 (2014) 66–76.
- [56] W. Yang, S.E. Naleway, M.M. Porter, M.A. Meyers, J. McKittrick, The armored carapace of the boxfish, Acta Biomater 23 (2015) 1–10.
- [57] W. Yang, H. Quan, M.A. Meyers, R.O. Ritchie, Arapaima fish scale: one of the toughest flexible biological materials, Matter (2019), doi:10.1016/j.matt.2019. 09.014
- [58] F.G. Torres, D. De la Torre, M. Merino, Dynamic mechanical analysis of fish dermal armour from A. gigas and P. pardalis, Bioinspired, Biomim. Nanobiomater (2015). doi:10.1680/bbn.15.00002.
- [59] J.D. Currey, Bones: structure and mechanics, Princeton University Press, Woodstock, United Kingdom, 2006.
- [60] L. Mulder, J.H. Koolstra, J.M. den Toonder, T.M. van Eijden, Relationship between tissue stiffness and degree of mineralization of developing trabecular bone, J. Biomed. Mat. Res. Part A 84 (2) (2008) 508–515.
- [61] A.P. Summers, J.H. Long Jr., Skin and bones, sinew and gristle: the mechanical behavior of fish skeletal tissues, Fish Physiol 23 (2005) 141–177.
- [62] W. Raschi, C. Tabit, Functional aspects of placoid scales: a review and update, Aust. J. Mar. Freshw. Res. 43 (1992) 123–147.
- [63] T.Y. Wu, Fish swimming and bird/insect flight, Annu. Rev. Fluid Mech. 43 (2011) 25–58.
- [64] D. Stuart-Fox, A. Moussalli, Camouflage, communication and thermoregulation: lessons from colour changing organisms, Philos. Trans. R. Soc. Biol. Sci. 364 (2009) 463–470.
- [65] B.G. Lovegrove, The evolution of body armor in mammals: plantigrade constrains of large body size, Evol. 55 (2001) 1464–1473.